http://dx.doi.org/10.5012/bkcs.2012.33.7.2435

Growth of ZnO Nanostructures by the Reaction of ZnO Powder with Carbon Monoxide

Sang-Won Seo and Woo-Sik Jung*

School of Chemical Engineering, College of Engineering, Yeungnam University, Gyongsan 712-749, Korea
**E-mail: wsjung@yu.ac.kr*
Received March 14, 2012, Accepted April 19, 2012

Key Words : Zinc oxide, Nanostructures, Carbon monoxide

Wurtzite-type zinc oxide (ZnO) is a promising semiconductor material with a wide bandgap of 3.3 eV at room temperature. Recently, ZnO nanostructures have attracted great research interest because of their simplicity in fabrication, variety in morphology, and diversity of application.[1,2] Until now, the methodologies known for growth of ZnO nanostructures have included metal organic chemical vapor deposition,[3,4] solution-based process,[5] and vapor phase transport (VPT).[6-11] The VPT process, in which Zn,[6,7] ZnO,[8] and a mixture of ZnO and carbon[9-14] are used as sources, has been the most frequently used for synthesizing a variety of ZnO nanostructures. For the carbothermal reduction using a mixture of ZnO and carbon powders, Zn vapors formed in the temperature range between 800 and 1200 °C are transported *via* a carrier gas onto a substrate and deposited as a thin film or nanostructures of ZnO on the substrate at lower temperatures.[9-14] Despite of the many studies on the carbothermal reduction, doubt remains as to how Zn vapor is oxidized to ZnO vapor during its transportation to the substrate. Two oxidants, oxygen (O_2) and carbon monoxide (CO), will be considered in the conversion of Zn to ZnO. The CO gas can be generated by the reaction of carbon with O_2.

In this work, we fabricated ZnO nanostructures on the substrate by the VPT process in which ZnO powder was heated under a flow of CO and demonstrated the plausibility of the oxidation of Zn vapor to ZnO vapor by CO. To the best of our knowledge, this is the first report of the fabrication of ZnO nanostructures by the reaction of ZnO powder with CO. Our previous paper showed that β-Ga_2O_3 nanobelts were obtained by the reaction of β-Ga_2O_3 powder and CO.[15]

ZnO powder in an alumina crucible was heated at 750 °C for 3 h in a gas mixture of nitrogen (N_2) and 1 vol % CO (hereafter referred to as 1 vol % CO/N_2). The reaction temperature used in this study was lower than that[9-14] in the carbothermal reduction method. Zn vapor generated by the reduction of ZnO powder by CO at a hot zone is oxidized to ZnO vapor and then deposited on the substrate away from the crucible:

$$ZnO\,(s) + CO\,(g) \rightarrow Zn\,(g) + CO_2\,(g) \text{ at a hot zone} \quad (1)$$

$$Zn\,(g) + CO\,(g) \rightarrow ZnO\,(g) + C\,(g, s) \quad (2)$$

$$ZnO\,(g) \rightarrow ZnO \text{ nanostructures on a substrate} \quad (3)$$

The substrate used in this study was fluorine-doped tin oxide (FTO) glass applicable to dye-sensitized solar cells. Photoelectrode films with nanostructured ZnO are known to significantly enhance solar-cell performance.[16] As shown in Figure 1(a), the colors of the as-grown products on the FTO glass gradually changed from black to greyish with increasing distance from the glass to the source. The deposited glass was classified into three zones according to the color. The temperature of each zone at the glass decreased along the gas flow direction. The morphologies of the ZnO nanostructures were determined by the distance, as done in other studies.[7,14] The product deposited at zone A above 530 °C consisted of irregularly shaped ZnO particles. Nanobelts and nanowires were grown at zone B, while hexagonal nanorods with a diameter of *ca.* 100 nm and nanocones were grown at zone C. The growth of crystals with different morphologies from the vapor phase is explained by the vapor-liquid mechanism, where the degree of vapor supersaturation is one of the factors determining the prevailing growth morpho-

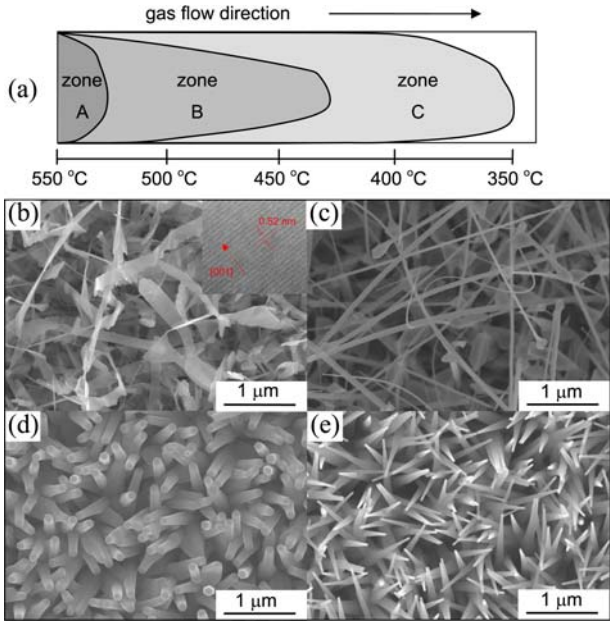

Figure 1. (a) Schematic division of products deposited on the FTO glass along the gas flow direction and (b-e) SEM images of (b) nanobelts, (c) nanowires, (d) nanorods, and (e) nanocones. The inset in Figure 1(b) shows an HRTEM image of the nanobelt.

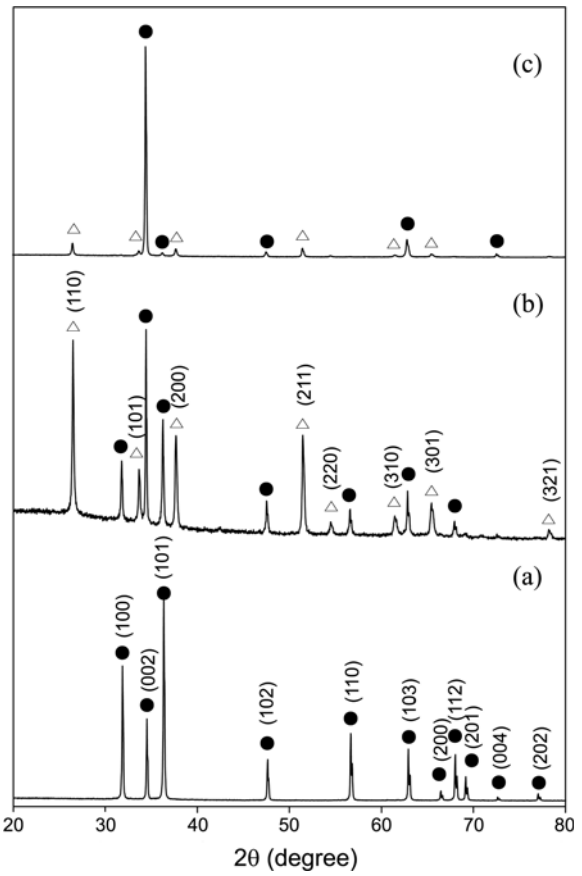

Figure 2. XRD patterns of ZnO nanostructures deposited on the FTO glass by calcination of ZnO powder at 750 °C for 3 h under a flow of 1 vol % CO/N_2. (a) powder, (b) nanobelts and nanowires, and (c) nanorods and nanocones. (●) ZnO, (△) FTO.

logy.[14,17] The degree depends on the temperature because the rate of reaction (2) is a function of the temperature. Zone A was under a very high supersaturation which caused the formation of poorly crystallized crystal with irregular morphology. A medium supersaturation facilitated the growth of nanobelts and nanowires, as shown in Figures 1(b) and 1(c). The inset in Figure 1(b) is a high resolution transmission electron microscopy (HRTEM) image of the nanobelt, showing that the lattice spacing of 0.52 nm corresponds to the *d*-spacing of (0002) planes of the wurtzite-type ZnO.[14] The nanorods and nanocones at zone C were grown under a low supersaturation, as shown in Figures 1(d) and 1(e). X-ray diffraction (XRD) patterns of the nanostructures deposited at zones B and C were measured and compared with that (Figure 2(a)) of wurtzite-type ZnO powder. Their patterns (Figures 2(b) and (c)) exhibited the most intense (002) diffraction peaks, indicating that the preferred growth direction of all nanostructures is [0001].

Raman scattering spectra were measured at room temperature to investigate the vibrational properties of the ZnO nanostructures grown at each zone, as shown in Figure 3. The Raman spectra of the nanostructures exhibited four main modes: $E_{2H\text{-}2L}$, A_1(TO), E_{2H}, and E_1(LO).[18] Two peaks at 436 and 329 cm^{-1} were assigned to E_{2H} and $E_{2H\text{-}2L}$ modes, respectively. The A_1(TO) mode was observed at 378 cm^{-1}

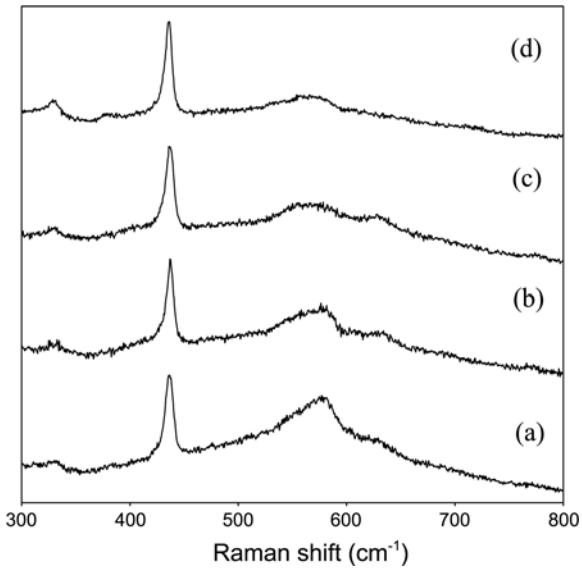

Figure 3. Raman spectra of (a) ZnO nanocones, (b) nanorods, (c) nanowires, and (d) nanobelts deposited on the FTO glass by calcination of ZnO at 750 °C for 3 h under a flow of 1 vol % CO/N_2.

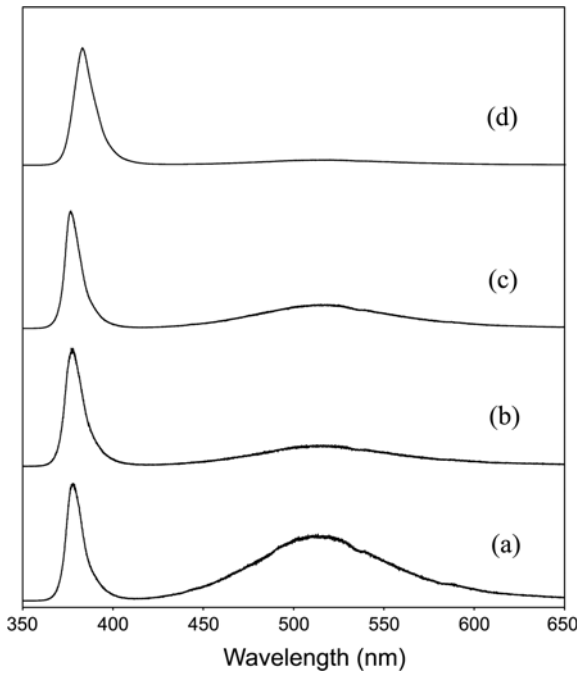

Figure 4. PL spectra of (a) ZnO nanocones, (b) nanorods, (c) nanowires, and (d) nanobelts deposited on the FTO glass by calcination of ZnO at 750 °C for 3 h under a flow of 1 vol % CO/N_2.

only for nanobelts. The E_1(LO) mode at 580 cm^{-1} for nanocones was the most intense among the nanostructures, indicating that the nanocones have the most non-stoichiometric defects such as Zn interstitials or oxygen vacancies.[6,13] The nanostructures grown at the lower temperature zone were expected to have more defects because of the slower rate of reaction (2).

Figure 4 shows the photoluminescence (PL) spectra of the ZnO nanostructures grown at each zone. The spectra

exhibited two bands: near band-edge (NBE) and defect-related emission. The NBE band appeared at 382 and 377 nm for nanobelts and the other nanostructures, respectively. Wang *et al.* showed that the NBE band for narrower nanobelts is blue-shifted due to a quantum effect.[1,19] The defect-related emission band, *i.e.*, green band, centered at 510 nm, which is attributed to the non-stoichiometric defects,[20] was extremely weak for nanobelts and the most intense for nanocones. The defect-related emission band was correlated to the E_1(LO) mode in the Raman spectra.

In order to determine whether or not Zn is oxidized to ZnO by CO according to reaction (2), Zn powder was calcined at 700 °C for 3 h under a flow of 10 vol % CO/N_2. The calcination resulted in the formation of ZnO and carbon. However, the amount of carbon, as determined by a CHN elemental analyzer, was too small to give conclusive evidence on the reaction between Zn and CO. Considering that Fe particles act as catalysts to fabricate carbon nanostructures with gaseous carbon,[21] a mixture of Zn and nanosized Fe (99.5%, Sigma-Aldrich) powders (50: l by weight ratio) was calcined at 700 °C for 3 h under a flow of 10 vol % CO/N_2. The XRD pattern (Figure 5(a)) of the product exhibited intense diffraction peaks of ZnO and Fe (ICDD-PDF #00-001-1252) together with a weak peak of graphite (ICDD-PDF #00-001-0640). As shown in Figure 5(b), the latter peak became intense after treatment of the product with 2 N HCl solution for 24 h. The appearance of a very weak peak assigned to Fe_2O_3 (ICDD-PDF #00-016-0653) in Figure 5(b) was attributed to the oxidation of Fe during the acid treatment because results on the calcination of only Fe powder 700 °C under a flow of 10 vol % CO/N_2 showed that Fe powder was inert to CO and that no carbonaceous material was formed. These results were considered to demonstrate that Zn is oxidized to ZnO by CO along with formation of carbon, as expressed in reaction (2).

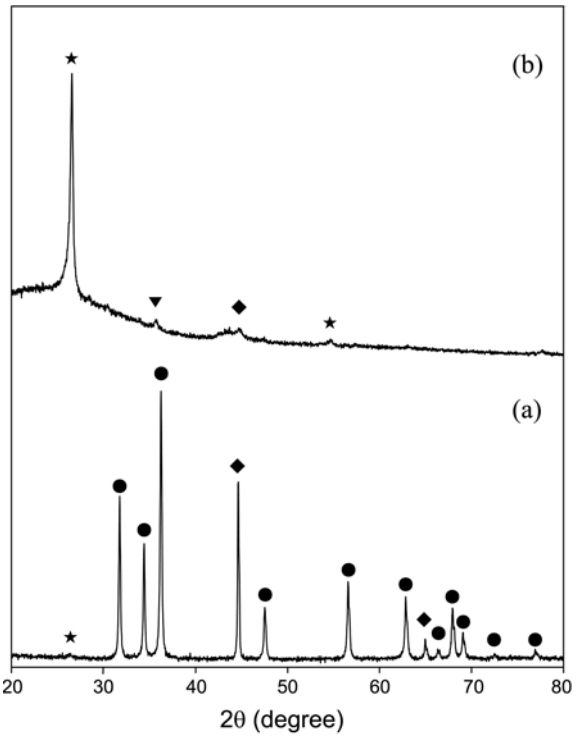

Figure 5. XRD patterns of samples obtained by calcination of a mixture of Zn and Fe at 700 °C for 3 h under a flow of 10 vol % CO/N_2: (a) before and (b) after acid treatment. (●) ZnO, (★) graphite, (◆) Fe, (▼) Fe_2O_3.

In conclusion, ZnO nanostructures were grown on FTO glass by VPT process in which ZnO powder is reduced to gaseous Zn and then oxidized to gaseous ZnO by CO. The morphologies of the ZnO nanostructures, the preferred growth orientation of which was along the *c*-axis, varied with the distance from the source to the substrate. The nanostructures grown at lower temperatures had more non-stoichiometric defects, as identified by Raman and PL spectra. This study demonstrated that CO partial pressure is a factor determining the morphologies of ZnO nanostructures in their growth by the carbothermal reduction.

Experimental Section

ZnO powder (99.99%, Sigma-Aldrich) in an alumina crucible was located at the center of an alumina tube with an inner diameter of 33 mm. The tube was placed inside a temperature-gradient horizontal furnace. The substrate of 2.5 cm × 7.0 cm FTO glass was positioned 20 cm downstream from the crucible. The crucible was heated to 750 °C at a rate of 5 °C/min in 1 vol % CO/N_2 gas flowing at 100 mL/min. The tube was cooled to room temperature under a flow of 1 vol % CO/N_2. As-grown products on the FTO glass were characterized by powder XRD (PANalytical X'Pert PRO MPD X-ray diffractometer with Cu-Kα radiation operating at 40 kV and 30 mA). The morphology and structure were examined by scanning electron microscopy (SEM; Hitachi S-4800) and HRTEM (Philips CM 200 STEM, working at 200 kV). Raman and PL spectra were measured at room temperature using the 514.5 nm line of an Ar^+ laser and the 325 nm line of an He-Cd laser (Jobin-Yvon LabRam HR spectrophotometer), respectively. The carbon content in the products was determined by a CHN elemental analyzer (Flash 1112, Thermo Fischer Scientific).

Acknowledgments. This work was supported by the Human Resources Development Program of Korea Institute of Energy Technology Evaluation and Planning (KETEP) grant (No. 20104010100580) funded by the Korean Ministry of Knowledge Economy.

References

1. Wang, Z. L. *J. Phys.: Condens. Matter* **2004**, *16*, R829.
2. Ahmad, M.; Zhu, J. *J. Mater. Chem.* **2011**, *21*, 599.
3. Choi, Y.-J.; Park, J.-H.; Park, J.-G. *J. Mater. Res*. **2005**, *20*, 959.
4. Kim, D. C.; Mohanta, S. K.; Cho, H. K. *Cryst. Growth Des*. **2009**, *9*, 4725.
5. Zhang, X. L.; Qiao, R.; Qiu, R.; Kim, J. C.; Kang, Y. S. *Cryst. Growth Des*. **2009**, *9*, 2906.
6. Umar, A.; Karunagaran, B.; Kim, S. H.; Suh, E.-K.; Hahn, Y. B. *Inorg. Chem.* **2008**, *47*, 4088.

7. Han, X.; Wang, G.; Jie, J.; Choy, W. C. H., Luo, Y.; Yuk, T. I.; Hou, J. G. *J. Phys. Chem. C* **2005**, *109*, 2733.
8. Shi, J.; Hong, H.; Ding, Y.; Yang, Y.; Wang, F.; Cai, W.; Wang, X. *J. Mater. Chem.* **2011**, *21*, 9000.
9. Chen, R.; Tay, Y.; Ye, J.; Zhao, Y.; Xing, G.; Wu, T.; Sun, H. *J. Phys. Chem. C* **2010**, *114*, 17889.
10. Yang, P.; Yan, H.; Mao, S.; Russo, R.; Johnson, J.; Saykally, R.; Morris, N.; Pham, J.; He, R.; Choi, H.-J. *Adv. Funct. Mater.* **2002**, *12*, 323.
11. Park, J.-H.; Choi, H.-J.; Choi, Y.-J.; Sohn, S.-H.; Park, J.-G. *J. Mater. Chem.* **2004**, *14*, 35.
12. Zhang, Z.; Wang, S. J.; Yu, T.; Wu, T. *J. Phys. Chem. C* **2007**, *111*, 17500.
13. Geng, C.; Jiang, Y.; Yao, Y.; Meng, X.; Zaipien, J. A.; Lee, C. S.; Lifshitz, Y.; Lee, S. T. *Adv. Funct. Mater.* **2004**, *14*, 589.
14. Ye, C.; Fang, X.; Hao, Y.; Teng, X.; Zhang, L. *J. Phys. Chem. B* **2005**, *109*, 19758.
15. Jung, W.-S. *Bull. Korean Chem. Soc*. **2006**, *27*, 1963.
16. Zhang, Q.; Dandeneau, C. S.; Zhou, X.; Cao, G. *Adv. Mater.* **2009**, *21*, 4087.
17. Campbell, W. B. *Whisker Technology*; Wiley-Interscience: New York, U.S.A., 1970; Chap. 2.
18. Damen, T. C.; Porto, S. P. S.; Tell, B. *Phys. Rev.* **1966**, *142*, 570.
19. Wang, X.; Ding, Y.; Summers, C. J.; Wang, Z. L. *J. Phys. Chem. B* **2004**, *108*, 8773.
20. Liu, X.; Wu, X.; Cao, H.; Chang, R. P. H. *J. Appl. Phys.* **2004**, *95*, 3141.
21. Liu, S.; Tang, X.; Mastai, Y.; Felner, I.; Gedanken, A. *J. Mater. Chem.* **2000**, *10*, 2502.